Microstructure evolution influenced by dislocation density gradients modeled in a reaction-diffusion system

Hallberg, Håkan; Ristinmaa, Matti

Published in:
Computational Materials Science

DOI:
10.1016/j.commatsci.2012.09.016

2013

Computational Materials Science 2013, 67(373-383)

Microstructure evolution influenced by dislocation density gradients modeled in a reaction-diffusion system

Håkan Hallberg*, Matti Ristinmaa
Division of Solid Mechanics
Lund University, Box 118, S-221 00 Lund, Sweden
*hakan.hallberg@solid.lth.se

Abstract

Macroscopic properties of metallic materials are to a large extent dictated by the grain size and the presence and arrangement of grain boundaries. Plastic slip deformation will lead to the formation of dislocation pile-ups at grain boundaries, causing a heterogeneous distribution of dislocation density. This will on the macroscale manifest itself as a grain size dependence of the yield stress. Considering dynamic recrystallization, new grains will nucleate at sites of high stored energy. The existence of such favored nucleation sites is also largely due to a heterogeneous dislocation density distribution. To properly account for processes such as these in microstructure modeling, dislocation density gradients and grain boundary influence need to be considered. In the present contribution, the evolution of dislocation density is viewed as a reaction-diffusion system, involving mobile and immobile dislocations. Gradient effects are introduced by making the immobilization of mobile dislocations sensitive to the distance to grain boundaries. Through simulations of both single grains and polycrystals, it is shown that the present model provides a macroscopic yield stress behavior of Hall-Petch type, without explicitly incorporating a yield stress dependence on the grain size. In addition, the model is employed in a cellular automaton algorithm, allowing a polycrystalline microstructure to evolve due to dynamic recrystallization. It is shown that the introduced gradients provide important additions to recrystallization modeling.

Keywords: Gradient effects, Dislocation density, Grain boundaries, Hall-Petch, Recrystallization, Modeling, Cellular automata

DOI: 10.1016/j.commatsci.2012.09.016

1 Introduction

Many important aspects of the macroscopic material behavior in metals are controlled by the microlevel grain structure. Strength and ductility depends largely on the size and distribution of the grains. Especially the presence of grain boundaries plays an important role, not least in the macroscopic deformation hardening of the material. Grain boundaries pose obstacles to slip deformation by preventing dislocation motion, resulting in localized dislocation storage and heterogeneous deformation fields within the grains. Dislocation density gradients have been observed in experiments, e.g. on Aluminum bi-crystals in [1], on Copper in [2], on dual-phase steels in [3] and on polycrystalline Ti6Al4V in [4].

The dislocation structure at grain boundaries facilitates lattice compatibility across the boundaries [5] and has led to the distinction between geometrically necessary dislocations (GND) in the vicinity of grain boundaries and the statistically stored dislocations (SSD) in the grain interiors [6].

The dislocation storage at grain boundaries increases as the area fraction of grain boundaries increase, i.e. as the average grain size decreases. This is the mechanism behind the well-established Hall-Petch effect, suggesting a proportionality between the macroscopic yield stress and the inverse of the square root of the average grain size [7, 8]. The Hall-Petch effect has been verified experimentally and its validity holds over a wide range of grain sizes, reaching down to the sub-micron scale [9]. However, at very fine grain sizes, the Hall-Petch relation is less applicable since grain boundary effects become appreciable throughout the grains.

Continuum models considering different dislocation species are frequent in the literature. A separation of mobile and (nearly) immobile, or forest, dislocations are made in [10, 11, 12, 13, 14, 15, 16, 17]. Three types of dislocation densities, immobile dislocations within dislocation cells and mobile/immobile dislocations in the cell walls are distinguished in [18, 19]. Dislocation density gradients are also considered on a continuum-level in [20, 21, 22]. Gradient effects due to inhomogeneous distribution of plastic slip and dislocation accumulation at grain boundaries have also been considered in crystal plasticity models, e.g. [23, 24], mainly aiming at retrieving a Hall-Petch effect in the homogenized macroscopic yield stress. Different dislocation species and their role in interface accommodation is studied in a crystal plasticity model of martensitic phase transformation in [25].

Reaction-diffusion modeling of dislocation density was originally considered in [26] and later employed in [27] and in the series of papers [28, 29, 30] on dislocation patterning, cf. also [31, 32, 33, 34, 35, 36]. Dislocation density gradients, evolving through a reaction-diffusion process, is considered in a crystal plasticity setting in [37]. The focus of the work in [37] lies on simulation of plastic slip behavior and dislocation interaction with grain boundaries in an idealized single crystal.

To the knowledge of the authors, there exist no reaction-diffusion models where dislocation density gradients are studied in conjunction with recrystallization and grain growth, being the dominant mechanisms for grain size evolution in metallic materials [38]. This is addressed in the present work.

A mesoscale model of microstructure evolution is established where a distinction is made between the densities of mobile and immobile dislocations. The two dislocation species are allowed to evolve through a reaction-diffusion process, driven by macroscopic deformation. Dislocation density gradients are introduced by making the reaction-diffusion system sensitive to the presence of grain boundaries, increasing dislocation immobilization as grain boundaries are approached and effectively modeling dislocation pile-ups at the boundaries. The model is employed in simulations of dislocation density evolution in both single grains and polycrystals and the homogenized macroscopic flow stress exhibits the expected grain size dependence in both cases.

Cellular automata provide a versatile and widely used tool in materials science for simulating microstructure evolution in terms of e.g. phase transformation, solid state precipitation, dendrite growth during solidification of melts, spherulite growth in polymers and recrystallization. Cellular automata modeling of recrystallization has been studied by several authors, e.g. [39, 40, 41, 42, 43, 44, 45]. Static recrystallization is simulated in a coupled crystal plasticity/cellular automaton algorithm in [46]. A cellular automaton algorithm was used for modeling of diffusion in [47] and for reaction-diffusion processes in [48, 49].

However, none of these models consider dislocation density gradients or dislocation interaction at grain boundaries. In [50], a cellular automaton formulation is adopted where the dislocation density within each grain is said to vary from the grain center to the boundary. No details on how the distribution is achieved are given.

In the present work, grain boundaries are assumed impenetrable to dislocations as a simplifying view of the dislocation absorption, emission and transmission that has been observed at grain boundaries in experiments [51, 52, 53]. This is achieved by prescribing a zero flux of dislocations across the grain boundaries. Dislocation migration across grain boundaries can, however, be incorporated in the present model and will be the subject of forthcoming studies.

To represent increased storage and immobilization of dislocations as the grain boundaries are approached, the reaction term whereby mobile dislocations are immobilized due to interaction with forest dislocations, is taken as a function of the distance to the grain boundary. By this formulation, immobilization of mobile dislocations accelerates in the vicinity of grain boundaries. The resulting heterogeneous distribution of dislocation densities and how it influences the macroscopic flow stress behavior is scrutinized as well as its effect on grain boundary migration behavior and nucleation of recrystallized nuclei.

The polycrystal model is formulated in a cellular automaton setting and a methodology

for treating the dislocation density gradients due to grain boundaries is introduced. The combination of a finite difference scheme for the evolution of dislocation densities and a cellular automaton formulation for the evolution of microstructure topology results in an efficient hybrid algorithm for mesoscale modeling of grain microstructures.

The present paper is divided into section. In Section 2, the dislocation density evolution laws and the components of the dislocation reaction-diffusion system are discussed. The gradient terms in the dislocation reactions are also introduced in this section. In Section 3, it is shown that the proposed model of dislocation density evolution in the grain interiors results in a variation of the macroscopic yield stress with grain size as predicted by the Hall-Petch relation, without explicitly including the grain size in the calculation of the yield stress. Instead, the size dependence enters the formulation on the microlevel through a length parameter related to the dislocation density gradients. Section 4 discusses the extension of the model to represent polycrystals. The 2D case is shown, noting that the extension to 3D is straight-forward. Simulations using the polycrystal model is related in Section 5. A Hall-Petch behavior of the flow stress is retrieved also in the case of polycrystals and it is shown how the Hall-Petch formulation looses in validity as very small grains are considered, where grain boundary effects dominate throughout the grain interiors. Prior to simulation of dynamic recrystallization, Section 6 summarizes the necessary equations for recrystallization modeling. Some further notes on the cellular automaton implementation are given in Section 7 and simulation of microstructure evolution during dynamic recrystallization is performed in Section 8. Finally, some concluding remarks are given in Section 9.

2 Evolution of dislocation densities

The dislocation density is assumed to be comprised of the density of mobile dislocations ρ_{m} and the density of (nearly) immobile dislocations ρ_{i}. The two populations are here assumed to evolve according to a reaction-diffusion process where the two types of dislocations are allowed to react with each other and each type is allowed to diffuse through the crystal structure, presently viewed as a continuous media. Following [27, 31], the balance equation for each type of dislocation density is given by

$$\begin{aligned} \frac{\partial \rho_{\mathrm{m}}}{\partial t} + \nabla \boldsymbol{j}_{\mathrm{m}} &= \left[p_{\mathrm{m}} \left(\rho_{\mathrm{m}}, \rho_{\mathrm{i}} \right) + q_{\mathrm{m}} \left(\rho_{\mathrm{m}}, \rho_{\mathrm{i}} \right) \right] \dot{\varepsilon}^{\mathrm{p}}_{\mathrm{eff}} \\ \frac{\partial \rho_{\mathrm{i}}}{\partial t} + \nabla \boldsymbol{j}_{\mathrm{i}} &= \left[p_{\mathrm{i}} \left(\rho_{\mathrm{m}}, \rho_{\mathrm{i}} \right) + q_{\mathrm{i}} \left(\rho_{\mathrm{i}} \right) \right] \dot{\varepsilon}^{\mathrm{p}}_{\mathrm{eff}} \end{aligned} \tag{1}$$

where ∇ is the divergence operator and $\boldsymbol{j}_{\mathrm{m,i}}$ the fluxes of mobile and immobile dislocations, respectively. Eqs. (1) renders a scalar description of the evolution of the dislocation densities and macroscopic material behavior will later on be considered in terms of J_2 plasticity.

The fluxes in eqs. (1) are given by

$$\begin{aligned} \nabla \boldsymbol{j}_{\mathrm{m}} &= -D_{\mathrm{m}} \nabla \rho_{\mathrm{m}} \\ \nabla \boldsymbol{j}_{\mathrm{i}} &= -D_{\mathrm{i}} \nabla \rho_{\mathrm{i}} \end{aligned} \tag{2}$$

where $D_{\mathrm{m,i}}$ is the diffusion coefficient of each type of dislocation species, satisfying $D_{\mathrm{m}} \gg D_{\mathrm{i}}$, cf. [27, 28, 14, 36].

Note that the terminology "diffusion coefficients" is used here in order to be consistent with the reaction-diffusion approach. In the present application, however, these coefficients rather measures the mobility of moving dislocation than diffusion of matter.

The right-hand sides of eqs. (1) are in the present model allowed to depend on the rate of macroscopic effective plastic strain $\dot{\varepsilon}^{\mathrm{p}}_{\mathrm{eff}}$, where a superposed dot denotes differentiation with respect to time t. Such slip rate dependence is also considered in [33, 54, 17]. The dependence on $\dot{\varepsilon}^{\mathrm{p}}_{\mathrm{eff}}$ is motivated by both generation of dislocations, e.g. due to Frank-Read sources, and dynamic recovery being dependent on the amount of plastic slip deformation in the material. Based on the model in [12], the coupling terms $p_{\mathrm{m,i}}$ in eqs. (1) are cast in the form

$$\begin{aligned} p_{\mathrm{m}}\left(\rho_{\mathrm{m}}, \rho_{\mathrm{i}}\right) &= -k_2 \rho_{\mathrm{m}} - k_3 \sqrt{\rho_{\mathrm{i}}} \\ p_{\mathrm{i}}\left(\rho_{\mathrm{m}}, \rho_{\mathrm{i}}\right) &= k_2 \rho_{\mathrm{m}} + k_3 \sqrt{\rho_{\mathrm{i}}} \end{aligned} \tag{3}$$

where conservation of the dislocation density is satisfied by $p_{\mathrm{m}} + p_{\mathrm{i}} = 0$ in the absence of the terms $q_{\mathrm{m,i}}$ in eqs. (1). The parameter k_2 controls the decrease of mobile dislocation density due to interaction between mobile dislocations and the term with the coefficient k_3 governs the immobilization of mobile dislocations with the mean free path being proportional to $\sqrt{\rho_{\mathrm{i}}}$, e.g. at cell walls. The density of mobile dislocations in eq. (1) is further influenced by a production term

$$q_{\mathrm{m}}\left(\rho_{\mathrm{m}}, \rho_{\mathrm{i}}\right) = k_1 \frac{\rho_{\mathrm{i}}}{\rho_{\mathrm{m}}} \tag{4}$$

where the k_1-parameter is related to dislocation generation from immobile dislocation sources. Similarly, the density of immobile dislocations in eq. (1) evolves under the influence of a dynamic recovery term

$$q_{\mathrm{i}}\left(\rho_{\mathrm{i}}\right) = -k_4 \rho_{\mathrm{i}} \tag{5}$$

where the extent of dynamic recovery of immobile dislocations due to processes of climb and cross-slip is controlled by the parameter k_4. The form of the production component in eq. (4) and of the dynamic recovery component in eq. (5) is based on the model in [12].

The total dislocation density, measuring the stored energy in the material, is taken as the sum of the mobile and immobile dislocation densities, i.e.

$$\rho = \rho_{\mathrm{m}} + \rho_{\mathrm{i}} \tag{6}$$

To introduce dislocation density gradients in the vicinity of the grain boundaries, the fluxes in eq. (2) are assumed to be zero at the grain boundaries and the parameter k_3 in eq. (3) is allowed to vary with the distance l to the boundary, i.e.

$$k_3 = k_3(l) \tag{7}$$

This formulation represents the physical processes of increased immobilization and storage of dislocations as the grain boundary is approached, which in the present model is assumed to be impenetrable for mobile dislocations. Transmission of dislocations across the grain boundaries can be incorporated into the present formulation by prescribing non-zero fluxes of dislocations across the boundaries. Grain boundaries, allowing dislocation transmission, are considered in a crystal plasticity model in [55].

The explicit form of the l-dependence in eq. (7) is chosen as

$$k_3(l) = k_{3,\max} - (k_{3,\max} - k_{3,\min})\, g(l) \tag{8}$$

where

$$g(l) = 1 - \exp(-wl), \quad l \geq 0 \tag{9}$$

From eqs. (8) and (9) it is apparent that the k_3 parameter is allowed to vary between a maximum $k_{3,\max}$ at the boundaries and a minimum $k_{3,\min}$ in the grain interior. The parameter w in eq. (9) controls how far into the grain interior the boundary influence should reach, cf. Fig. 1. Lacking experimental data on values pertaining to this length parameter, it is heuristically chosen in the present study. Setting $k_{3,\min} = 0$ prevents immobilization of mobile dislocations due to interaction with immobile dislocations within the grains, a distance away from the boundary.

A length scale, similar to the present l, is introduced in the crystal plasticity model in [56] where a distinction is made between statistically stored and geometrically necessary dislocation species. The size dependence of the model enters due to the presence of geometrically necessary dislocations.

The function $g(l)$ in eq. (9) is discussed further in the 2D polycrystal formulation in Section 4.

2.1 One-dimensional case study

To illustrate the behavior of the dislocation reaction-diffusion equations in eq. (1), a one-dimensional grain of diameter d is studied. To account for boundary effects at each end of the one-dimensional domain, eq. (9) is made symmetric around $l = d/2$ according to

$$\widetilde{g}(l) = 1 - \exp(-wl) - \exp(-w(l-d)), \quad 0 \leq l \leq d \tag{10}$$

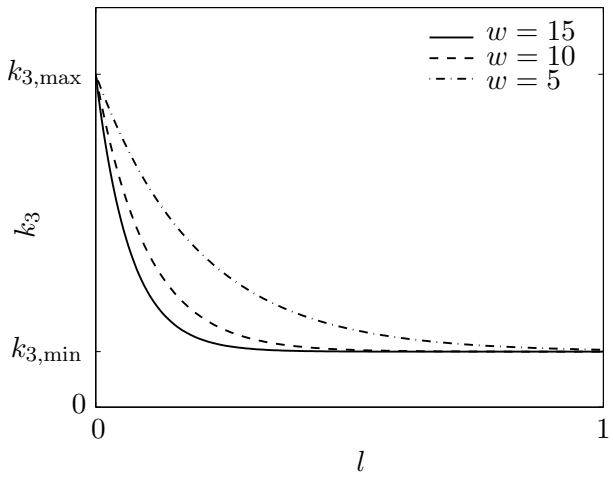

Figure 1: Variation of the k_3 parameter from the grain boundary, where $l = 0$, towards the grain center. The different lines show the effect of varying the parameter w in eq. (9).

and with consequent notation the k_3-parameter appears as $\widetilde{k}_3$. For illustration purposes, the parameters in the dislocation density evolution laws are chosen according to [12], giving $k_1 = 3.1 \times 10^{14}$ m^{-2}, $k_2 = 5.5$, $\widetilde{k}_{3,\max} = 4.2 \times 10^7$ m^{-1} and $k_4 = 6.7$. For simplicity $\widetilde{k}_{3,\min} = 0$ is set. A strain rate of $\dot{\varepsilon}^{\mathrm{p}}_{\mathrm{eff}} = 1 \times 10^{-2}$ s^{-1} is assumed. The diffusion coefficients D_{m} and D_{i} are set to $D_{\mathrm{m}} = 1 \times 10^{-12}$ m^2/s and $D_{\mathrm{i}} = 1 \times 10^{-14}$ m^2/s. The initial densities of mobile and immobile dislocations are set as $\rho^0_{\mathrm{m}} = 1 \times 10^{10}$ m^{-2} and $\rho^0_{\mathrm{i}} = 1 \times 10^{10}$ m^{-2}, respectively. It can be noted that, as also observed in [12], the influence of initial dislocation densities on subsequent dislocation density evolution is negligible.

Eqs. (1) are solved using an explicit finite difference scheme with a centered difference approximation in space and a forward Euler approximation in time. The one-dimensional domain under consideration is given by $0 \leq l \leq d$, where d is the grain size. Zero-flux boundary conditions are prescribed at $l = 0$ and $l = d$. The parameter w in eq. (10) is set to $w = 15$, cf. Fig. 1. In the numerical solution, the spatial domain $0 \leq l \leq d$ is divided into 100 segments and a grain size of $d = 1$ μm is used.

The effect of varying the grain size d is shown in Fig. 2. These graphs show the varying influence of the grain boundary gradients as the grain size change. The results are obtained at a total macroscopic effective plastic strain of $\varepsilon^{\mathrm{p}}_{\mathrm{eff}} = 0.5$. In the numerical scheme, the spatial discretization is varied to keep the segment length Δl fixed at 0.01 μm, i.e. to maintain the same spatial resolution for all grain sizes under consideration. From Fig. 2 it is evident that the grain boundaries will have an increasing influence on the distributions of dislocation densities as the grain size is reduced. This is closely related to the Hall-Petch effect, considered in the following section.

Fig. 3 shows the average dislocation densities as a function of macroscopic effective

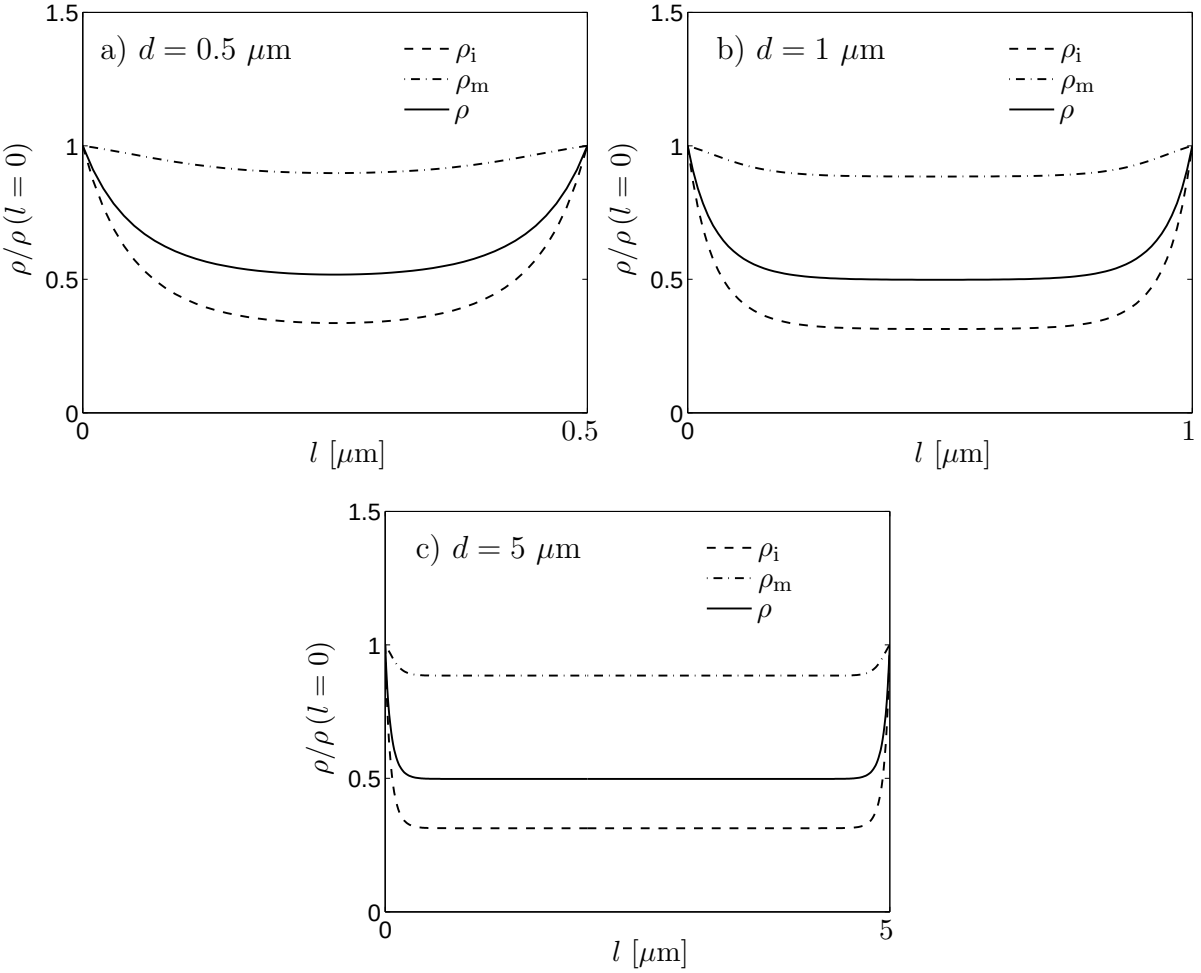

Figure 2: Distribution of dislocation density in grains of different diameter d at an effective plastic strain of $\varepsilon^{\mathrm{p}}_{\mathrm{eff}} = 0.5$. Note that the individual dislocation densities are normalized by their values at $l = 0$: a) $d = 0.5$ μm, b) $d = 1$ μm and c) $d = 5$ μm.

plastic strain, obtained from the one-dimensional calculations using the stated parameter values and a grain size of $d = 1$ μm.

3 Hall-Petch relation obtained from one-dimensional calculations

Classically, the relation between the macroscopic yield stress and the average grain size of a material is given by the Hall-Petch relation [7, 8], indicating a proportionality between this yield stress $\bar{\sigma}_{\mathrm{y}}$ and the inverse of the square root of the average grain size, i.e.

$$\bar{\sigma}_{\mathrm{y}} = \bar{\sigma}_{\mathrm{y0}} + \frac{\bar{k}}{\sqrt{d}} \tag{11}$$

where $\bar{\sigma}_{\mathrm{y0}}$ and $\bar{k}$ are parameters.

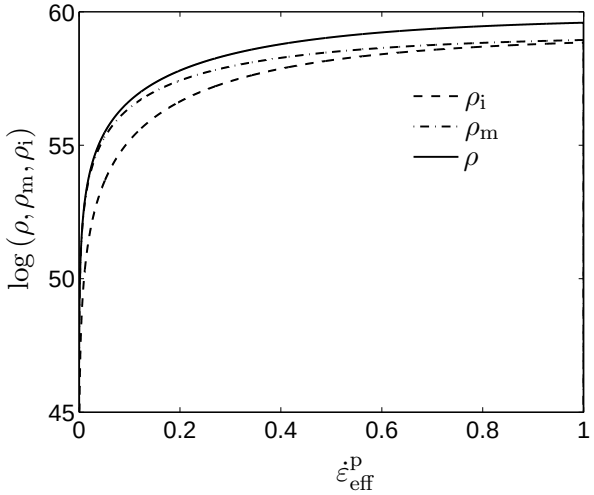

Figure 3: Average dislocation densities in a one-dimensional grain with diameter $d = 1$ μm as functions of macroscopic effective plastic strain.

The Hall-Petch relation is usually demonstrated based on the variation of the initial yield stress with average grain size. It has, however, been shown that a corresponding grain size dependence is valid for arbitrary deformation states after initial yielding [57, 58, 59, 60]. In this view, the parameters $\bar{\sigma}_{\mathrm{y}0}$ and $\bar{k}$ are constants for a given value of strain.

The relation in eq. (11) is a manifestation of the increasing interaction between grain boundaries and dislocations as the grain size is reduced, i.e. as the area fraction of grain boundaries increases. By this reasoning, the Hall-Petch relation should be recovered in the present study as an effect of considering dislocation density gradients, influenced by the presence of grain boundaries.

To retrieve the Hall-Petch effect from the present dislocation density-based model, J_2 plasticity is assumed and the macroscopic yield stress is taken as a function of the average, total, dislocation density $\langle\rho\rangle$ according to

$$\sigma_\mathrm{y} = \sigma_{\mathrm{y}0} + \alpha\mu b\sqrt{\langle\rho\rangle} \tag{12}$$

where $\sigma_{\mathrm{y}0}$ is the Peierls' stress needed to overcome lattice friction, μ is the shear modulus, b is the magnitude of the Burgers vector and α a constant.

Using the one-dimensional model, described in the previous section, the average dislocation density is calculated for different grain sizes. The corresponding yield stress values are obtained from eq. (12) by assuming $\sigma_{\mathrm{y}0} = 200$ MPa, $\mu = 77$ GPa, $b = 0.3$ nm and $\alpha = 0.5$, which are values representative for steel. The results are plotted in Fig. 4 as circles. These results are shown together with a solid line, representing the Hall-Petch relation in eq. (11). The parameter values $\bar{\sigma}_{\mathrm{y}0} = 239.6$ MPa and $\bar{k} = 0.01$ MPa$\cdot$m$^{1/2}$ were obtained by a least squares fitting procedure.

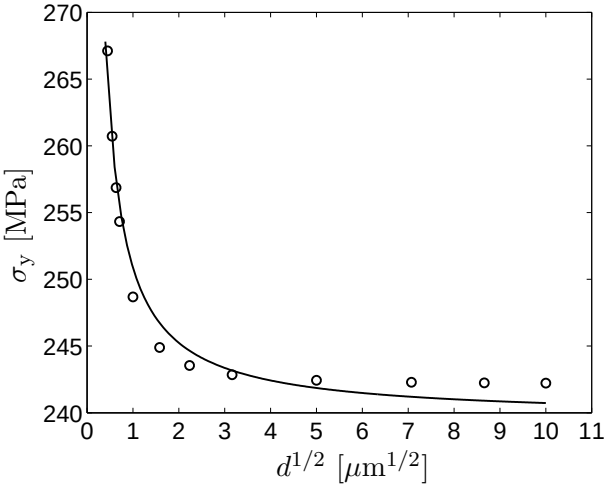

Figure 4: Variation of the macroscopic yield stress with the square-root of the grain size $d^{1/2}$. Results obtained from one-dimensional calculations at $\varepsilon^{\mathrm{p}}_{\mathrm{eff}} = 0.25$, and using eq. (12), are shown as symbols and the solid line shows the fitted Hall-Petch relation in eq. (11).

From Fig. 4, it is seen that the one-dimensional calculations result in a grain size-dependence of the macroscopic yield stress that agrees well with the Hall-Petch relation.

The present modeling approach, with dislocation density gradients and viewing the evolution of dislocation densities as a reaction-diffusion system, is capable of representing the effect of reduced grain size on the macroscopic flow stress behavior without explicitly including the grain size as is done in the Hall-Petch formulation. Instead, the grain size-dependence enters naturally as dislocation interaction with grain boundaries is taken into account. In fact, the present results, as shown in Fig. 2, are in close agreement with the original works by Hall and Petch, cf. [7, 8], and also by Cottrell [61]. In these papers, the Hall-Petch effect is explained in terms of dislocation pile-ups at the grain boundaries that cause stress concentrations at, or slightly ahead of, the dislocation pile-up.

4 Model formulation for polycrystals

To investigate the behavior of the reaction-diffusion model of dislocation densities in the case of polycrystalline materials, a 2D microstructure is considered in this section. The 2D case is used for simplicity although it is noted that extension to 3D is straight-forward. Again, an explicit finite difference scheme is used for the evolution of the dislocation densities. The scheme is applied to an RVE described by a fixed two-dimensional grid with dimensions 512×512 μm and a total of 1024×1024 grid divisions.

As the present dislocation model will be applied to cellular automata modeling of dynamic recrystallization in subsequent sections, the notion of each grid point being a

"cell" is introduced at this stage. To each cell belongs a number of state variables. For the present purpose, the state variables consist of the cell's density of mobile and immobile dislocations, respectively, and an identifying number stating to which grain the cell belongs. With the RVE dimensions just stated, each cell will have a side-length of $l_c = 0.5$ μm. Periodic boundary conditions are applied at the boundaries of the domain.

In the polycrystal formulation, microstructure evolution is described by a cellular automaton algorithm, except for the evolutions of the dislocation densities which are obtained by employing a finite difference scheme on the cellular automaton cell grid. In this section, grain boundaries are set to remain fixated and immobile to allow studying the effects of the reaction-diffusion dislocation density model alone. In later sections the migration of grain boundaries and nucleation of new grains due to dynamic recrystallization will be considered in a cellular automaton formulation. Additional details on the cellular automaton implementation are given in Section 8.

A Taylor assumption is presently made, whereby the deformation is viewed as being equal in all grains. Macroscopic flow stress behavior is assumed to obey standard J_2 plasticity.

The 2D microstructure is viewed as a cross-section of the corresponding 3D polycrystalline material. This allows the average diameter of grain i to be calculated as

$$\bar{d}_i = 2l_c\sqrt{\frac{n_{\text{cell},i}}{\pi}} \tag{13}$$

where $n_{\text{cell},i}$ is the number of cells belonging to grain i.

In eq. (7), the immobilization of mobile dislocations due to interaction with immobile dislocations, in terms of the parameter k_3, was made dependent on the distance l to the grain boundary by introducing the function $g(l)$. To keep track of the distance of each cell in a single grain, relative to the grain boundary, a distance number n_{dist} is assigned to the individual cells. The boundary cells of the grains are identified and are given the distance number 1. All cells within the grain, having a neighbor with distance number 1 are subsequently given the distance number 2 and so on. This is continued until all cells are numbered, cf. Fig. 5. When recrystallization with migrating grain boundaries and appearance/disappearance of grains are considered later on, the distance numbers have to be recalculated in each time step.

Based on the distance numbers, the distance l in eq. (7) is identified as an integer number of cells n_l defining the distance from the boundary – where $n_l = 1$, cf. Fig. 5 – and the function $k_3(l)$ in eqs. (8) and (9) is recast in the form

$$k_3(n_l) = k_{3,\max} - (k_{3,\max} - k_{3,\min})\left(1 - \exp\left[-w\left(n_l - 1\right)\right]\right), \quad n_l \geq 1 \tag{14}$$

In this form, eq. (14) satisfies $k_3 = k_{3,\max}$ at the boundary where $n_l = 1$ and $k_3 = k_{3,\min}$ a distance away from the boundary, indirectly determined by the parameter w. The behavior of eq. (14) is illustrated in Fig. 6 for different values of w.

The macroscopic yield stress is obtained from the cellular automaton RVE by considering

$$\sigma_{\mathrm{y}} = \sigma_{\mathrm{y0}} + \alpha\mu b\sqrt{\bar{\rho}} \tag{15}$$

where the homogenized dislocation density is obtained from

$$\sqrt{\bar{\rho}} = \frac{1}{V}\sum_{g}\int_{V_g}\sqrt{\rho_g}dV \tag{16}$$

In this expression, V is the total RVE volume and V_g and ρ_g are the volume and total dislocation density of grain g, respectively. The summation is performed over all grains. This homogenization procedure is discussed further in [45].

5 Polycrystal simulations

Initial microstructures with different grain sizes are generated by allowing different numbers of nuclei to grow until they impinge upon each other under purely curvature-driven motion. Such grain growth kinetics are further discussed in Section 6. Some of the microstructures used are shown in Fig. 7. In total, 20 different microstructures with average grain sizes ranging between 2 μm and 111 μm are employed.

The k_i-parameters in the dislocation density evolution equations, cf. eqs. (3)-(5), are set to the same values as was used previously in Section 2. Also the strain rate of $\dot{\varepsilon}^{\mathrm{p}}_{\mathrm{eff}} = 1\times10^{-2}$ s^{-1} and the diffusion coefficients $D_{\mathrm{m}} = 1\times10^{-12}$ m^2/s and $D_{\mathrm{i}} = 1\times10^{-14}$ m^2/s are maintained as well as the initial densities of mobile and immobile dislocations which are

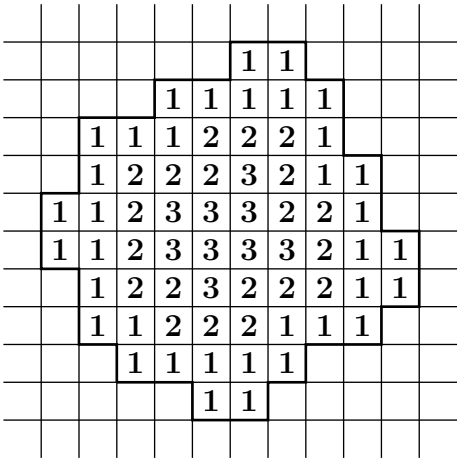

Figure 5: Schematic illustration of the use of distance numbers to keep track of a how far the cells in a grain are from the grain boundary. The grain boundary is indicated by a thick line.

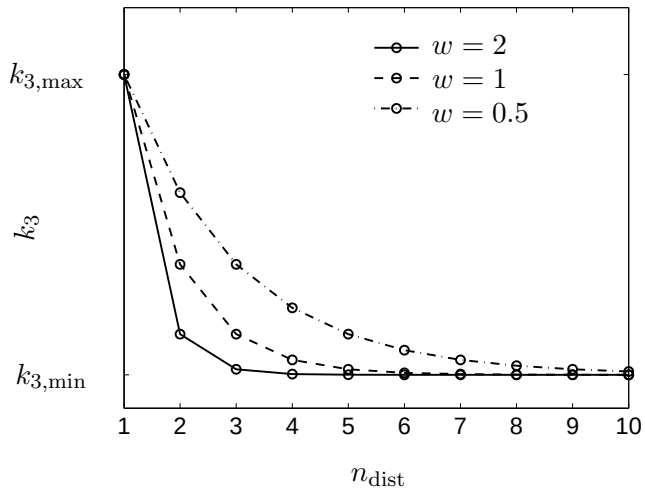

Figure 6: Variation of the k_3-parameter within a grain in the computational cell grid using the distance numbers n_{dist}. Note that the lines are only shown to indicate the trends since in the cell grid, each value of n_{dist} represents an individual cell in which k_3 attains a constant value.

homogeneously set as $\rho_{\text{m}}^0 = 1 \times 10^{10}$ m^{-2} and $\rho_{\text{i}}^0 = 1 \times 10^{10}$ m^{-2} to represent the annealed initial state.

The discrete variation in one dimension of the parameter k_3 is illustrated schematically in Fig. 6 for different values of w. The same variations of k_3 are also illustrated in a 2D polycrystal with 75 grains in Fig. 8.

From Fig. 8 it is obvious that as the value of w is reduced, the dislocation density gradient protrudes deeper into the grains and the boundary effects become increasingly influential in the grain interiors, cf. Fig. 8a. For small grains, and small values of w, boundary effects will dominate throughout the grain. Correspondingly, higher values of w sharpens the dislocation density gradient and the gradient-affected region of the grains lies close to the grain boundaries, cf. Fig. 8d.

The different microstructures are utilized with the present reaction-diffusion model to simulate the evolution of dislocation densities up to a total strain of $\varepsilon_{\text{eff}}^{\text{p}} = 0.5$. Fig. 9 shows the resulting, homogenized, flow stress for some of the grain sizes under consideration when $w = 0.1$. As expected, an increased flow stress can be observed in Fig. 9 as smaller grain sizes are considered.

In Fig. 9, it is worth noting that the flow curves have the same origin, regardless of grain size. This is due to all simulations starting with a homogeneous dislocation density distribution without any gradients. This has been chosen as a modeling assumption since a qualitative study is performed, instead of postulating some initial heterogeneity.

The variation of the flow stress with grain size at $\varepsilon_{\text{eff}}^{\text{p}} = 0.25$ is shown in Fig. 10 for the

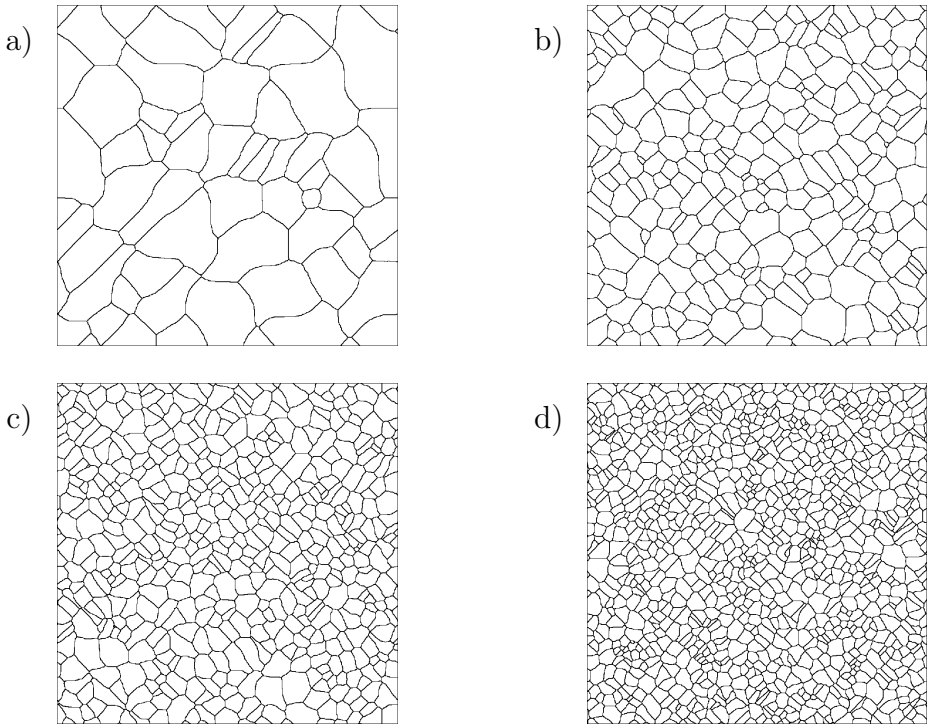

Figure 7: Examples of the microstructures used in the present simulations. The microstructures have different average grain size: a) 78 μm (50 grains), b) 35 μm (250 grains), c) 25 μm (500 grains) and d) 18 μm (1000 grains).

different values of the parameter w also considered in Fig. 8. In Fig. 10, symbols represent simulation results and the solid lines represent the Hall-Petch relation in eq. (11).

From the results in Fig. 10, it can be noted that as $w = 0.1$ is employed, grain boundary effects tend to dominate far into the grain interior, cf. Fig. 8a. Consequently, the simulation results in Fig. 10 deviate significantly from a Hall-Petch type of behavior as smaller grain sizes are considered. This is in fact a manifestation of how the Hall-Petch formulation is less applicable as the grain size is reduced, i.e. as boundary effects prevail throughout the grain interiors. However, as the value of w is increased and the dislocation density gradients near the grain boundaries become steeper – i.e. as dislocation pile-ups are more confined to a region close to the boundaries – the simulation results in Fig. 10 more closely follows a typical Hall-Petch behavior. The solid lines in Fig. 10 are fitted to the simulation results through a least-squares procedure, resulting in $\bar{\sigma}_{\mathrm{y0}} = 243.6$ MPa and $\bar{k} = 52.7$ MPa$\cdot$m$^{1/2}$ for $w = 0.5$, $\bar{\sigma}_{\mathrm{y0}} = 240.9$ MPa and $\bar{k} = 52.0$ MPa$\cdot$m$^{1/2}$ for $w = 1$ and $\bar{\sigma}_{\mathrm{y0}} = 239.9$ MPa and $\bar{k} = 50.3$ MPa$\cdot$m$^{1/2}$ for $w = 2$.

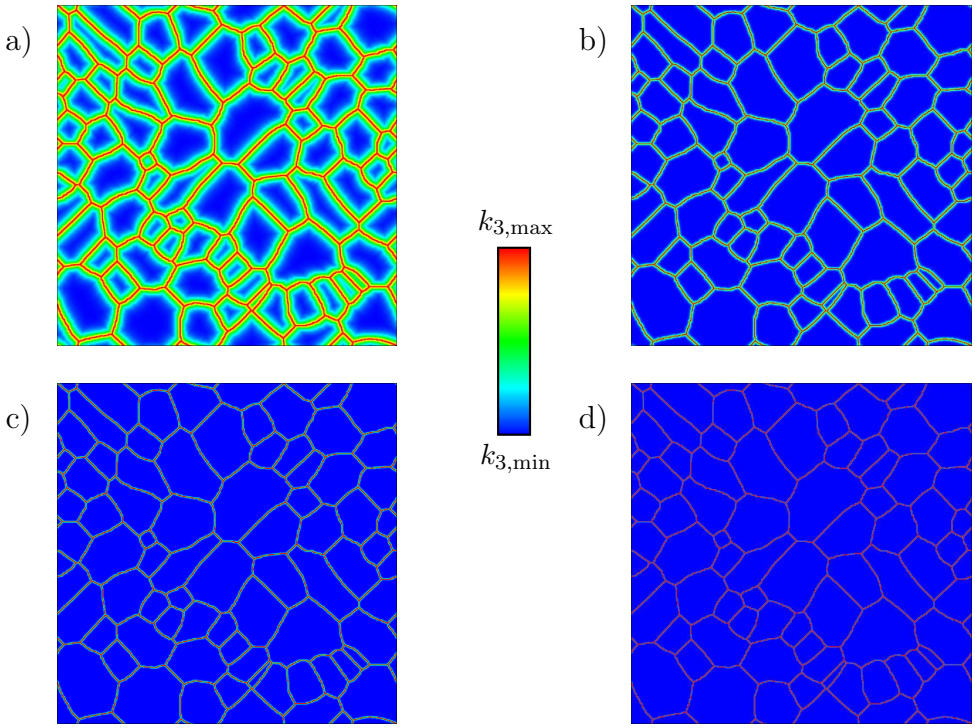

Figure 8: Variation of the k_3 parameter in a 2D microstructure with 75 grains and an average grain size of $d = 64$ μm. The different figures are obtained by different choices of the parameter w: a) $w = 0.1$, b) $w = 0.5$, c) $w = 1$ and d) $w = 2$.

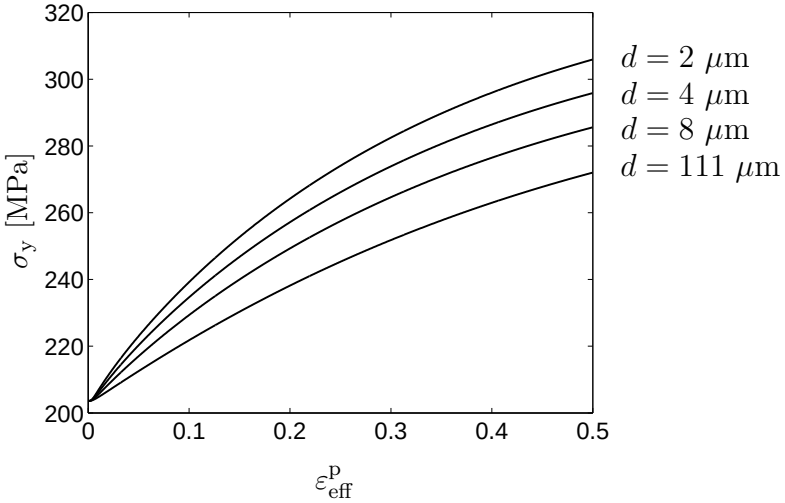

Figure 9: Homogenized flow stress obtained from the polycrystal simulations for some different grain sizes and with $w = 0.1$.

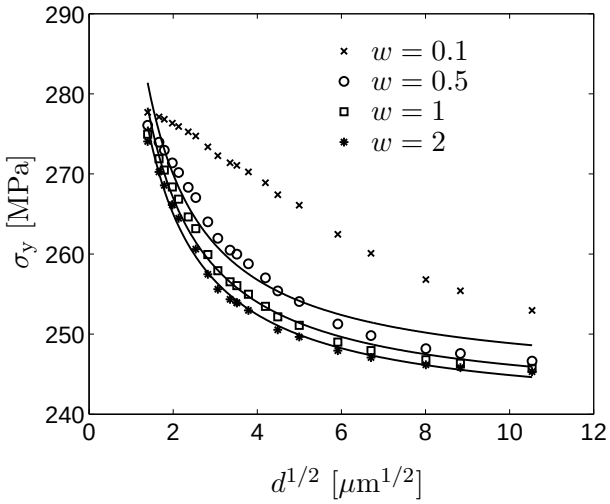

Figure 10: Variation of the flow stress, obtained at $\varepsilon^{\mathrm{p}}_{\mathrm{eff}} = 0.25$, for different grain sizes and for different values of the w-parameter, corresponding to the values used in Fig. 8. Symbols represent simulation results and solid lines least-squares fittings of the Hall-Petch relation in eq. (11).

6 Recrystallization kinetics

Prior to applying the proposed model to a cellular automata simulation of recrystallization, the necessary recrystallization kinetics need to be established.

Considering dynamic discontinuous recrystallization, i.e. recrystallization driven by plastic deformation and proceeding by nucleation and growth of new grains, the rate of nucleation per unit grain boundary length is chosen as

$$\dot{n} = c\dot{\varepsilon}^{\mathrm{p}}_{\mathrm{eff}} \exp\left(-\frac{Q_{\mathrm{n}}}{RT}\right) \tag{17}$$

where Q_{n} is the activation energy for nucleation, R the gas constant and T the absolute temperature, a constant parameter in the present isothermal study. The activation energy Q_{n} can be a function of local conditions of e.g. stored energy, but is here taken as a constant for simplicity. The coefficient c is generally a temperature dependent material parameter, but is presently set as a constant parameter as isothermal conditions are assumed. This parameter is further discussed in relation to the calibration of the model below.

The local migration velocity of a grain boundary, directed along the boundary normal, has the format

$$v = mp \tag{18}$$

where m is the mobility and p the driving pressure, taken as

$$p = \tau\left[\rho\right] - 2\gamma\kappa \tag{19}$$

The dislocation line tension is here denoted by $\tau = \mu b^2/2$, the jump in total dislocation density across a grain boundary by $[\rho]$ and the grain boundary energy by γ. The local boundary curvature κ is approximated, based on the cellular automaton grid discretization, as discussed later on.

The grain boundary mobility, appearing in eq. (18), may depend on both temperature T and relative crystallographic misorientation θ across the boundary. Following [62, 38, 63, 64, 65], the mobility is taken as

$$m\left(T,\theta\right) = m_0\left(T\right)\left[1-\exp\left\{-B\left(\frac{\theta}{\theta_{\mathrm{m}}}\right)^k\right\}\right]\exp\left(-\frac{Q_{\mathrm{m}}}{RT}\right) \tag{20}$$

where Q_{m} is the activation energy for grain boundary migration and $k = 4$ and $B = 5$ are parameters, chosen according to [62]. The shift from low-angle to high-angle boundaries is assumed to occur at $\theta_{\mathrm{m}} \approx 15°$. According to [65], the pre-exponential term in eq. (20) appears as

$$m_0\left(T\right) = \frac{\delta D_{\mathrm{GB}} b}{kT} \tag{21}$$

where δ is a typical grain boundary width, D_{GB} is the coefficient of grain boundary self diffusion and k the Boltzmann constant. Again, as isothermal conditions are considered, T as well as m_0 are treated as a constant parameters.

The grain boundary energy is here assumed to follow the Read-Shockley relation [66] for low-angle boundaries, where $\theta \leq \theta_{\mathrm{m}}$. For high-angle boundaries, the grain boundary energy is assumed to attain the constant value of γ_0, cf. [38]. In the present study, the grain boundary energy is thus taken as

$$\gamma\left(\theta\right) = \begin{cases} \gamma_0 \dfrac{\theta}{\theta_{\mathrm{m}}}\left[1-\ln\left(\dfrac{\theta}{\theta_{\mathrm{m}}}\right)\right] & \text{if} \quad \theta \leq \theta_{\mathrm{m}} \\ \gamma_0 & \text{if} \quad \theta > \theta_{\mathrm{m}} \end{cases} \tag{22}$$

The parameters in eq. (17) and in eqs. (20)-(22) are given in relation to calibration of the model, as shown later on.

7 Cellular automaton implementation

Having established the reaction-diffusion model of dislocation densities in a 2D polycrystal in previous sections, the cellular automaton implementation of the model can now be completed. One remaining issue is the local boundary curvature, first appearing in eq. (19). In the present cellular automaton implementation, this quantity is approximated by considering an expanded neighborhood to each cell as was used in [67, 45]. The curvature is

by this approach obtained from

$$\kappa = \frac{a_\kappa}{l_c} \frac{n_k - n_i}{n_c + 1} \tag{23}$$

where a_κ is a fitting parameter and l_c the side length of a cellular automaton cell. In the present case an expanded neighborhood containing the $n_c = 24$ nearest- and second-nearest neighbors is used. The number of cells within this expanded neighborhood that belongs to grain i is denoted by n_i and $n_k = 10$ is the number of cells in the expanded neighborhood that would represent a locally planar interface, giving $n_k = n_i$ and $\kappa = 0$. Following the procedure in [45] for calibration of the parameter a_κ in eq. (23), $a_\kappa = 3.5$ is obtained.

During a cellular automaton simulation, the size of the time step must be controlled with respect to the physical processes that are studied. In the case of recrystallization, the time step Δt is continuously adjusted to allow the fastest migrating grain boundary, with velocity $v_{\max}$, to advance a single cell distance l_c during a step. However, since the reaction-diffusion evolution of dislocation densities in the present model is solved by an explicit central difference scheme in the cellular automaton, an additional restriction is put on the allowable time step, given by the diffusion coefficients D_i and D_m. Noting that $D_\mathrm{m} \gg D_\mathrm{i}$, the time increment is in each step obtained from

$$\Delta t = \min \left(\frac{l_\mathrm{c}}{v_{\max}}, \frac{1}{2} \frac{l_\mathrm{c}^2}{D_\mathrm{m}} \right) \tag{24}$$

Following the approach in [45], a probabilistic cell state switching rule is used. In each time step, the maximum grain boundary velocity $v_{\max}$ occurring in the modeled polycrystal is calculated. Next, a switching probability $w_{\mathrm{switch}} = v/v_{\max}$ is calculated for all cells residing at grain boundaries, having the local migration velocities $v \leq v_{\max}$. A random number $\xi \in [0, 1]$ is generated for each of these cells and if $\xi \leq w_{\mathrm{switch}}$, the cell switch is accepted and otherwise it is rejected. This use of a probabilistic switching rules avoids the nonphysical situation where all migrating boundaries, having different velocities, would be allowed to advance during a common time step.

Further details of the cellular automaton algorithm are discussed in [45].

8 Cellular automata simulation of dynamic recrystallization

To perform simulations of dynamic recrystallization, the k_i-parameters previously used are employed again and additional parameter values are chosen in ranges pertaining to copper. It is noted that the values of the k_i-parameters are not necessarily representative for this material, but they are chosen for simplicity since a qualitative study is aimed for. The additional material parameters are summarized in Table 1, also cf. [45]. The parameter w is set to $w = 1$ and a process temperature of $T = 800$ K is assumed. This temperature

is within the range where dynamic recrystallization has been experimentally observed in pure copper, cf. [45].

The grains are given a random initial orientation from a uniform distribution in the interval between 0 and 90°, resulting in an isotropic orientation distribution.

Nucleation of new grains is initiated as the total dislocation density reaches a critical threshold value ρ_c. Once this condition is fulfilled, nucleation proceeds according to the nucleation rate defined by eq. (17). The dislocation density threshold value is in the present case taken as $\rho_c = 1 \times 10^{14}$ m^{-2} and the coefficient c in eq. (17) is set to $c = 2 \times 10^{21}$ m^{-2}.

Recrystallization nuclei are given random orientations from the same distribution as the original grains and the nuclei are also defined by zero initial dislocation densities.

By the above combination of chosen parameter values, and using an initial RVE microstructure with 150 grains and an average initial grain size of 45 μm, the flow stress behavior shown in Fig. 11 is obtained. Serrations in the flow stress occur due to repeated cycles of recrystallization in the microstructure [38, 45]. In the simulation, the initial grain size of 45 μm is reduced to a saturation value of 16 μm at the end of the deformation. A qualitatively similar behavior, exhibiting oscillatory flow stress as in Fig. 11 and grain refinement, can be observed in the experimental results on copper presented in [71].

The distribution of total dislocation density at the onset of recrystallization, cf. point A in Fig. 11, is shown in Fig. 12. The close-up view shows how the highest levels of dislocation density can be found at triple junctions followed by somewhat lower concentrations along grain boundaries. The dislocation density gradients gradually decline as one moves away from the grain boundaries and into the grain interiors where the dislocation density is considerably reduced.

The concentration of dislocation density at grain boundaries and primarily at triple junctions, illustrated in Fig. 12, has an important implication in recrystallization modeling. Nucleation of new grains occur at sites of high stored energy, i.e. of high dislocation density, and experiments locate the nucleation sites to triple junctions and grain boundaries [38].

The usual approach in simulation models of recrystallization – and particularly so in

Table 1: Material parameters entering the present model. The values are representative for pure Cu.

Parameter	Value	Description	Source
γ_0	0.625 J·m^{-2}	Grain boundary energy for HAGBs	[68]
δD_{GB}	5×10^{-15} m^{-3}/s	Grain boundary diffusivity	[69]
α	0.5	Dislocation interaction strength parameter	[63]
Q_m	104 kJ·mol^{-1}	Activation energy for grain boundary migration	[38]
b	0.256 nm	Magnitude of the Burgers vector	[70]
Q_n	261 kJ·mol^{-1}	Activation energy for nucleation	[71]
μ	28 GPa	Shear modulus	[68]

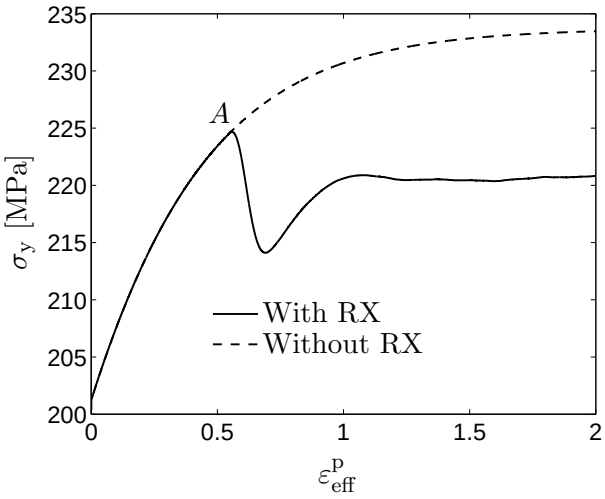

Figure 11: Flow stress behavior obtained from the cellular automaton simulation. The onset of recrystallization occurs at point A. Results from a simulation with recrystallization (RX) is shown by a solid line and results without recrystallization is shown by a dashed line.

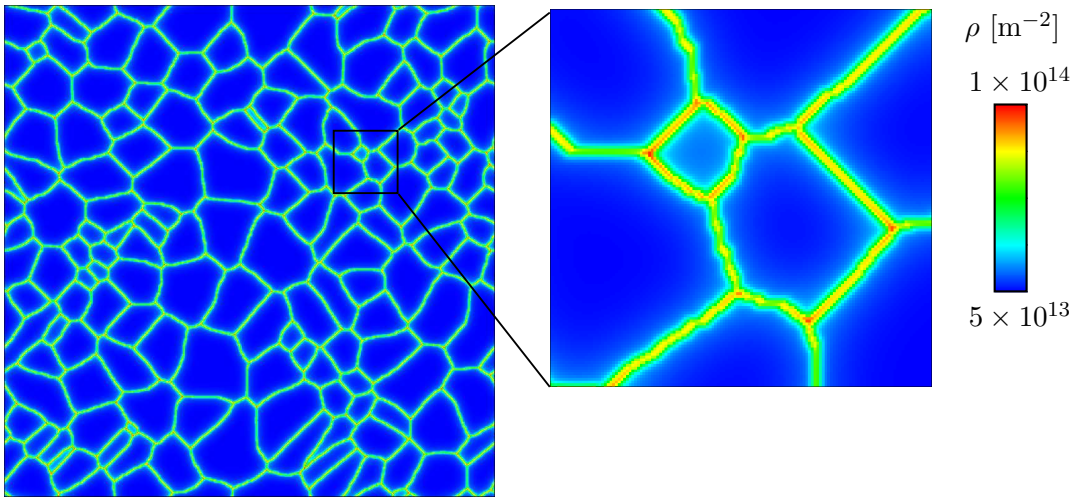

Figure 12: Distribution of total dislocation density at the onset of recrystallization, indicated as point A in Fig. 11. The close-up shows how the dislocation is concentrated primarily at triple junctions and secondly along grain boundaries.

cellular automata models – is to manually place the recrystallization nuclei at preferred sites in the microstructure. Using the present approach with dislocation density gradients, the nucleation sites emerge naturally without manual intervention.

Some stages of the microstructure evolution during the cellular automata simulation are

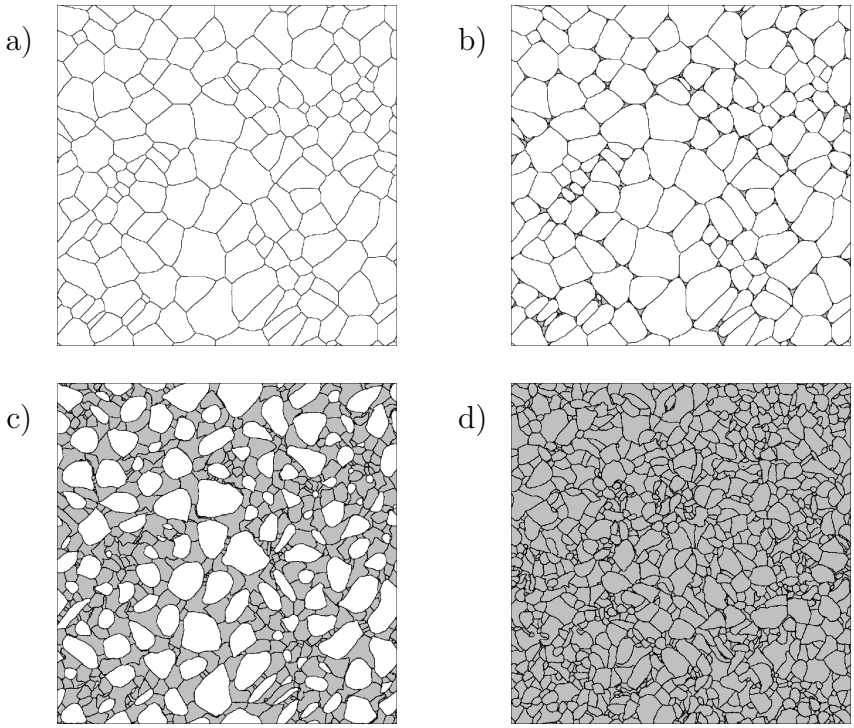

Figure 13: Microstructure at different deformation states, cf. Fig. 11a. Recrystallized grains are shaded gray. a) Initial microstructure with 150 grains and an average grain size of 45 μm at $\varepsilon^{\mathrm{p}}_{\mathrm{eff}} = 0$, b) Growth of the first nuclei from triple junctions at $\varepsilon^{\mathrm{p}}_{\mathrm{eff}} = 0.56$, c) Necklace pattern of recrystallized grains at $\varepsilon^{\mathrm{p}}_{\mathrm{eff}} = 0.63$ and d) Final grain structure with 977 grains and an average grain size of 16 μm at $\varepsilon^{\mathrm{p}}_{\mathrm{eff}} = 2$.

illustrated in Fig. 13. Recrystallized material is shaded gray. The first picture, Fig. 13a, shows the initial grain structure. The appearance of recrystallization nuclei is illustrated in Fig. 13b. After additional nucleation and growth, the recrystallized grains are localized along the grain boundaries of the initial microstructure, forming a necklace pattern, cf. Fig. 13c. The resulting recrystallized microstructure, at the end of the deformation process, is shown in Fig. 13d. At this point, the initial average grain size of 45 μm has been reduced to approximately 16 μm.

In addition to providing physically sound nucleation sites, the present model also influence the grain boundary migration rate. Recalling eq. (19), the driving pressure acting on a grain boundary is dependent on the jump in dislocation density across the boundary. With dislocation density gradients and dislocation pile-ups along the boundaries, a more physically realistic driving pressure is obtained than in the usual approach with a homogeneous dislocation density distribution.

9 Concluding remarks

To account for heterogeneous distributions of stored energy in grain microstructures, a model is established where mobile and immobile dislocations are allowed to evolve as a reaction-diffusion system. It is shown in the present work how dislocation density gradients can be introduced through the presence of grain boundaries. By this approach, one-dimensional calculations verify that a macroscopic flow stress with a Hall-Petch type of dependence on the grain size is obtained, without explicitly making the flow stress a function of the grain size. The size dependence enters the formulation on the microlevel through a length parameter related to the dislocation density gradients.

In addition, a methodology is established to introduce the dislocation density gradients in polycrystal simulations on the grain scale, using a fixed spatial grid for the numerical algorithm. This method is then applied to finite difference and cellular automata simulations of polycrystalline microstructures. Again, it is shown how the macroscopic, homogenized, flow stress exhibits a Hall-Petch variation with the average grain size of the microstructure. In addition, the polycrystal simulations illustrate how the Hall-Petch relation becomes less applicable for materials with very small grain sizes. In these cases, the interaction between dislocations and grain boundaries becomes influential throughout the microstructure, changing the flow stress dependence on grain size.

The polycrystal model is finally employed in a cellular automaton simulation of dynamic recrystallization and it is shown that the present formulation – involving dislocation density gradients – provide important additions to the common modeling approach where homogeneous dislocation density distributions are used. Due to the reaction-diffusion evolution of dislocation density, the stored energy level will be highest at triple junctions and along grain boundaries. This allows nucleation of recrystallization grains to occur spontaneously at those sites where experiments suggest, without having to manually specify suitable nucleation sites as is the usual approach in recrystallization simulations. It is also recognized that the presently introduced stored energy gradient will influence the migration velocity of mobile grain boundaries, altering recrystallization kinetics.

References

[1] S. Sun, B.L. Adams, and W.E. King. Observation of lattice curvature near the interface of a deformed aluminum bicrystal. *Phil. Mag. A*, 80(1):9–25, 2000.

[2] E. Demir, D. Raabe, N. Zaafarani, and S. Zaefferer. Investigation of the indentation size effect through the measurement of the geometrically necessary dislocations beneath small indents of different depths using EBSD tomography). *Acta Mater.*, 57:559–569, 2009.

[3] M. Calcagnotto, D. Ponge, E. Demir, and D. Raabe. Orientation gradients and geometrically necessary dislocations in ultrafine grained dual-phase steels studied by 2D and 3D EBSD. *Mater. Sci. Eng.*, A527:2738–2746, 2010.

[4] P.D. Littlewood, T.B. Britton, and A.J. Wilkinson. Geometrically necessary dislocation density distributions in Ti-6Al-4V deformed in tension. *Acta Mater.*, 59:6489–6500, 2011.

[5] J.F. Nye. Some geometrical relations in dislocated crystals. *Acta Metall. Mater.*, 1:153–162, March 1953.

[6] M.F. Ashby. The deformation of plastically non-homogeneous materials. *Phil. Mag.*, 21(170):399–424, 1970.

[7] E.O. Hall. The Lüders Deformation of Mild Steel. *Proc. R. Soc., London*, Section B(64):1085–1086, 1951.

[8] N.J. Petch. The Cleavage Strength of Polycrystals. *J. Iron Steel Inst.*, 174(1):25–28, 1953.

[9] M.E. Kassner, S. Nemat-Nasser, Z. Suo, G. Bao, J.C. Barbour, L.C. Brinson, H. Espinosa, H. Gao, S. Granick, P. Gumbsch, K.-S. Kim, W. Knauss, L. Kubin, J. Langer, B.C. Larson, L. Mahadevan, A. Majumdar, S. Torquato, and F. van Swol. New directions in mechanics. *Mech. Mater.*, 37:231–259, 2005.

[10] F.B. Prinz and A.S. Argon. The evolution of plastic resistance in large strain plastic flow of single phase subgrain forming metals. *Acta Metall. Mater.*, 32(7):1021–1028, 1984.

[11] D. Walgraef and E.C. Aifantis. Dislocation patterning in fatigued metals as a result of dynamical instabilities. *J. Appl. Phys.*, 58(2):688–691, 1985.

[12] Y. Estrin and L.P. Kubin. Local strain hardening and nonuniformity of plastic deformation. *Acta Metall. Mater.*, 34(12):2455–2464, 1986.

[13] H. Mughrabi. A two-parameter description of heterogeneous dislocation distributions in deformed metal crystals. *Mater. Sci. Eng.*, 85:15–31, 1987.

[14] C. Schiller and D. Walgraef. Numerical simulation of persistent slip band formation. *Acta Metall. Mater.*, 36(3):563–574, 1988.

[15] M.A. Zikry and M. Kao. Inelastic microstructural failure mechanicms in crystalline materials with high angle grain boundaries. *J. Mech. Phys. Solids*, 44(11):1765–1798, 1996.

[16] W.M. Ashmawi and M.A. Zikry. Grain boundary effects and void porosity evolution. *Mech. Mater.*, 35:537–552, 2003.

[17] J. Shi and M.A. Zikry. Grain-boundary interactions and orientation effects on crack behavior in polycrystalline aggregates. *Int. J. Solids Struct.*, 46:3914–3925, 2009.

[18] F. Roters, D. Raabe, and G. Gottstein. Work hardening in heterogeneous alloys – A microstructural approach based on three internal state variables. *Acta Mater.*, 48:4181–4189, 2000.

[19] F. Roters, P. Eisenlohr, L. Hantcherli, D.D. Tjahjanto, T.R. Bieler, and D. Raabe. Overview of constitutive laws, kinematics, homogenization and multiscale methods in crystal plasticity finite-element modeling: Theory, experiments, applications. *Acta Mater.*, 58:1152–1211, 2010.

[20] I. Groma, F.F. Csikor, and M. Zaiser. Spatial correlations and higher-order gradient terms in a continuum description of dislocation dynamics. *Acta Mater.*, 51:1271–1281, 2003.

[21] S. Yefimov, I. Groma, and E. van der Giessen. A comparison of a statistical-mechanics based plasticity model with discrete dislocation plasticity calculations. *J. Mech. Phys. Solids*, 52:279–300, 2004.

[22] M. Zaiser, N. Nikitas, T. Hochrainer, and E.C. Aifantis. Modelling size effects using 3D density-based dislocation dynamics. *Phil. Mag.*, 87:1283–1306, 2007.

[23] L.P. Evers, D.M. Parks, W.A.M. Brekelmans, and M.G.D. Geers. Crystal plasticity model with enhanced hardening by geometrically necessary dislocation accumulation. *J. Mech. Phys. Solids*, 50:2403–2424, 2002.

[24] M. Ekh, M. Grymer, K. Runesson, and T. Svedberg. Gradient crystal plasticity as part of the computational modelling of polycrystals. *Int. J. Numer. Meth. Eng.*, 72:197–220, 2007.

[25] J. Kundin, D.Raabe, and H.Emmerich. A phase-field model for incoherent martensitic transformations including plastic accommodation processes in the austenite. *J. Mech. Phys. Solids*, 59:2082–2102, 2011.

[26] D.L. Holt. Dislocation cell formation in metals. *J. Appl. Phys.*, 41(8):3197–3201, 1970.

[27] D. J. Bammann and E. C. Aifantis. On a proposal for a continuum with microstructure. *Acta Mech.*, 45:91–121, 1982.

[28] D. Walgraef and E.C. Aifantis. On the formation and stability of dislocation patterns - I: One-dimensional considerations. *Int. J. Eng. Sci.*, 23(12):1351–1358, 1985.

[29] D. Walgraef and E.C. Aifantis. On the formation and stability of dislocation patterns - II: Two-dimensional considerations. *Int. J. Eng. Sci.*, 23(12):1359–1364, 1985.

[30] D. Walgraef and E.C. Aifantis. On the formation and stability of dislocation patterns - III: Three-dimensional considerations. *Int. J. Eng. Sci.*, 23(12):1365–1372, 1985.

[31] E.C. Aifantis. On the dynamical origin of dislocation patterns. *Mater. Sci. Eng.*, 81:563–574, 1986.

[32] E.C. Aifantis. The physics of plastic deformation. *Int. J. Plasticity*, 3:211–247, 1987.

[33] A. Franěk, R. Kalus, and J. Kratochvíl. Model of early stage of dislocation structure formation in cyclically deformed metal crystals. *Phil. Mag. A*, 64(3):497–511, 1992.

[34] L.P. Kubin and G. Canova. The modelling of dislocation patterns. *Scripta Metall. Mater.*, 27:957–962, 1992.

[35] M.V. Glazov and C. Laird. Size effects of dislocation patterning in fatigued materials. *Acta Metall. Mater.*, 43(7):2849–2857, 1995.

[36] J.M. Salazar, R. Fournet, and N. Banai. Dislocation patterns from reaction-diffusion models. *Acta Metall. Mater.*, 43(3):1127–1134, 1995.

[37] A. Arsenlis, D.M. Parks, R. Becker, and V.V. Bulatov. On the evolution of crystallographic dislocation density in non-homogeneously deforming crystals. *J. Mech. Phys. Solids*, 52:1213–1246, 2004.

[38] F.J. Humphreys and M. Hatherly. *Recrystallization and related annealing phenomena*. Pergamon, New York, second edition, 2004.

[39] H.W. Hesselbarth and I.R. Göbel. Simulation of recrystallization by cellular automata. *Acta Metall. Mater.*, 39(9):2135–2143, 1991.

[40] C.H.J. Davies. The effect of neighbourhood on the kinetics of a cellular automaton recrystallization model. *Scripta Metall. Mater.*, 33(7):1139–1143, 1995.

[41] C.H.J. Davies. Growth of nuclei in a cellular automaton simulation of recrystallization. *Scripta Metall. Mater.*, 36(1):35–40, 1997.

[42] R.L. Goetz and V. Seetharaman. Modeling of dynamic recrystallization using cellular automata. *Scripta Metall. Mater.*, 38(3):405–413, 1998.

[43] D. Raabe. Cellular automata in materials science with particular reference to recrystallization simulation. *Annu. Rev. Mater. Res.*, 32:53–76, 2002.

[44] D. Raabe and L. Hantcherli. 2D cellular automaton simulation of the recrystallization texture of an IF sheet steel under consideration of Zener pinning. *Comp. Mater. Sci.*, 34:299–313, 2005.

[45] H. Hallberg, M. Wallin, and M. Ristinmaa. Modeling of discontinuous dynamic recrystallization in pure Cu using a probabilistic cellular automaton. *Comp. Mater. Sci.*, 49(1):25–34, 2010.

[46] D. Raabe and R. C. Becker. Coupling of a crystal plasticity finite-element model with a probabilistic cellular automaton for simulating primary static recrystallization in aluminium. *Modelling and Simulation in Materials Science and Engineering*, 8:445–462, 2000.

[47] B. Chopard and M. Droz. Cellular automata model for the diffusion equation. *J. Stat. Phys.*, 64(3-4):859–892, 1991.

[48] R. Kapral. Discrete models for chemically reacting systems. *J. Math. Chem.*, 6:113–163, 1991.

[49] J.R. Weimar. Cellular automata for reaction-diffusion systems. *Parallel Comput.*, 23:1699–1715, 1997.

[50] N. Yazdipour, C.H.J. Davies, and P.D. Hodgson. Microstructural modeling of dynamic recrystallization using irregular cellular automata. *Comp. Mater. Sci.*, 44:566–576, 2008.

[51] Z. Shen, R.H. Wagoner, and W.A.T. Clark. Dislocation and grain boundary interactions in metals. *Acta Metall. Mater.*, 36(12):3231–3242, 1988.

[52] T.C. Lee, I.M. Robertson, and H.K. Birnbaum. Interaction of dislocations with grain boundaries in Ni_3Al. *Acta Metall. Mater.*, 40(10):2569–2579, 1992.

[53] I. Baker and F. Liu. On *in-situ* study of dislocation/grain boundary interactions using X-ray topography and TEM. *Mat. Res. Soc. Symp. Proc.*, 319:203–214, 1994.

[54] J. Kratochvíl and M. Saxlová. Sweeping mechanisms of dislocation pattern formation. *Scripta Metall. Mater.*, 26:113–116, 1992.

[55] F. Roters A. Ma and D. Raabe. Studying the effect of grain boundaries in dislocation density based crystal-plasticity finite element simulations. *Int. J. Solids Struct.*, 43:7287–7303, 2006.

[56] F. Roters A. Ma and D. Raabe. A dislocation density based constitutive model for crystal plasticity FEM including geometrically necessary dislocations. *Acta Mater.*, 54:2169–2179, 2006.

[57] A.W. Thompson, M.I. Baskes, and W.F. Flanagan. The dependence of polycrystal work hardening on grain size. *Acta Metall. Mater.*, 21:1017–1028, 1973.

[58] M. Dollar and S. Gorczyca. The effect of grain size on polycrystal hardening. *Scripta Metall. Mater.*, 16:901–906, 1982.

[59] M. Dollar, J.M. Bernstein, and A.W. Thompson. Influence of deformation substructure on flow and fracture of fully pearlitic steel. *Acta Mater.*, 36(2):311–320, 1988.

[60] J.A. del Valle, F. Carreno, and O.A. Ruano. Influence of texture and grain size on work hardening and ductility in magnesium-based alloys processed by ECAP and rolling. *Acta Mater.*, 54:4247–4259, 2006.

[61] A.H. Cottrell. Theory of brittle fracture in steel and similar metals. *Trans. Met. Soc. AIME*, 212:192–203, 1958.

[62] F.J. Humphreys. A unified theory of recovery, recrystallization and grain growth, based on stability and growth of cellular microstructures - I. The basic model. *Acta Mater.*, 45(10):4231–4240, 1997.

[63] C. Zheng, N. Xiao, D. Li, and Y. Li. Mesoscopic modeling of austenite static recrystallization in a low carbon steel using a coupled simulation method. *Comp. Mater. Sci.*, 45:568–575, 2009.

[64] F. Montheillet, O. Lurdos, and G. Damamme. A grain scale approach for modeling steady-state discontinuous dynamic recrystallization. *Acta Mater.*, 57:1602–1612, 2009.

[65] G. Gottstein and L.S. Schvindlerman. *Grain Boundary Migration in Metals.* CRC Press, 2010.

[66] W.T. Read and W. Shockley. Dislocation models of crystal grain boundaries. *Phys. Rev.*, 78:275–289, 1950.

[67] K. Kremeyer. Cellular automata investigations of binary solidifications. *J. Comput. Phys.*, 142:243–262, 1998.

[68] H.S. Zurob, Y. Brechet, and J. Dunlop. Quantitative crietrion for recrystallization nucleation in single-phase alloys: Prediction of critical strains and incubation times. *Acta Mater.*, 54:3983–3990, 2006.

[69] H.J. Frost and M.F. Ashby. *Deformation-Mechanism Maps*. Pergamon Press, 1982.

[70] H.S. Kim, Y. Estrin, E.Y. Gutmanas, and C.K. Rhee. A constitutive model for densification of metal compacts: the case of copper. *Mater. Sci. Eng.*, 307:67–73, 2001.

[71] L. Blaz, T. Sakai, and J.J. Jonas. Effect of initial grain-size on dynamic recrystallization of copper. *Met. Sci.*, 17(12):609–616, 1983.